Radiation Physics and Chemistry 194 (2022) 110033

Contents lists available at ScienceDirect

Radiation Physics and Chemistry

journal homepage: www.elsevier.com/locate/radphyschem

Energy deposition by H and He ions at keV energies in self-supporting, single crystalline SiC foils

Eleni Ntemou *, Radek Holeňák, Daniel Primetzhofer

Department of Physics and Astronomy, Uppsala University, 751 20, Uppsala, Sweden

ARTICLE INFO

Keywords:
Silicon carbide (SiC)
keV ions
Transmission
Electronic stopping cross section

ABSTRACT

The specific energy deposition of H and He ions in SiC has been studied for both random and channeling orientations. The experiments were carried out in transmission geometry using the Time-of-Flight Medium Energy Ion Scattering System at the 350 keV Danfysik Implanter at Uppsala University. The target was a self-supporting, single crystalline cubic 3C–SiC (100) foil with nominal thickness of 200 nm. The measured stopping cross sections are compared with data available from the literature and theoretical predictions. The results for random geometries reveal slightly lower values than predicted by SRIM for H projectiles whereas for He projectiles good agreement was observed over the whole energy range studied. Higher specific energy loss is observed along random trajectories in comparison to channeling geometry, for all measured energies and for both H and He ions. For H ions, however, differences are minor, whereas for He ions, they are found generally more pronounced.

1. Introduction

The stopping power (dE/dx) is used to relate the energy lost by impinging ions to the distance travelled in the target material. Such energy loss experienced by the ions traversing matter is a consequence of inelastic collisions with the atomic electrons and elastic collisions with the atomic nuclei of the target material, referred to as electronic and nuclear stopping, respectively. The contribution of each one of these terms to the total energy loss depends mostly on the ion velocity and on the charge of ion and the target nuclei. At ion velocities significantly higher than the Bohr velocity of the atomic electrons ($v > v_0$), corresponding to the right side of the Bragg peak (Bragg and Kleeman, 1905), the electronic stopping is dominant and experimental stopping data are well predicted by the Bethe formula (Bethe, 1930) and corrections (Barkaset al., 1963; Andersenet al., 1977). At lower ion velocities (around v_0) nuclear stopping commonly becomes significant. However, for light ions such as H and He the electronic stopping power is dominant, even at keV energies. In this regime, where the solid is typically modelled by a free electron gas with constant density (Lindhard and Scharff (1953)), the electronic stopping is expected to be approximately proportional to the ion velocity (Wang and Nastasi). The transfer of energy of such slow ions, to the electronic system, however, is not yet completely understood since dynamic processes such as charge exchange and electron excitation and ionization in atomic collisions (Riccardiet al., 2017) become increasingly important and show a strong trajectory dependence (Lohmann and Primetzhofer, 2020; Primetzhoferet al., 2011a; Primetzhoferet al., 2013). In order to understand how and to which extend these fundamental processes contribute to target excitation, the energy deposition of ions traversing matter should be accurately known.

Also, in applied science and technology, knowing the energy loss per path length is a prerequisite for accurate materials characterization and modification based on energetic ions, e.g. in ion beam analysis, ion implantation, irradiation, sputtering and for hadron therapy (Duranteet al., 2017). Silicon carbide (SiC) is a material of high technological interest since it exhibits superior physical and electronic properties e.g. wide bandgap, high radiation tolerance and high thermal conductivity. Such properties render SiC an ideal material for use in high-temperature power electronics and in harsh environments e.g. high-voltage power devices, fusion devices or space applications (Roccaforteet al., 2018; Werneret al., 2001). SiC is used in dosimeters and radiation detectors due to the ability to operate in high radiation fields at room temperature (Puglisi and Bertuccio, 2019; Bruzziet al., 2001). For device applications, it is doped for the production of SiC-based devices (Hanet al., 2020; Vajdiet al., 2020), frequently implemented at nanoscale sizes in which the assessment and measurement of ionizing radiation dose (nanodosimetry) is necessary. In addition, there is ongoing research in the field of nuclear energy on

* Corresponding author.
E-mail address: eleni.ntemou@physics.uu.se (E. Ntemou).

https://doi.org/10.1016/j.radphyschem.2022.110033
Received 17 November 2021; Received in revised form 19 January 2022; Accepted 10 February 2022
Available online 11 February 2022

SiC-based nuclear fuel cladding materials in reactors (Zhanget al., 2021).

Data on the specific energy loss in SiC at ion energies below the Bragg maximum is, however, scarce and furthermore to large extend obtained in an indirect approach from a combination of ion implantation and secondary ion mass spectrometry experiments (Jansonet al., 2004; https://www-nds.iaea.org/). Moreover, since the energy loss is impact parameter dependent (Brandtet al., 1973), a necessity for specific energy loss measurements in different trajectories emerges. In order to address these issues, we present measurements of the specific energy loss for H and He ions in the energy range from 60 to 300 keV in SiC, for both random and channel orientations. The channeled ions traverse in a region of reduced electron density and hence, reduced stopping is expected as compared to the random orientation, furthermore complex excitation processes due to e.g. formation of molecular orbital, are reduced to a minimum. Apart from the applied relevance, providing experimental results for single-crystalline SiC (100) in a regime where the ion velocity is comparable with the velocities of the valence electrons could serve as a benchmark for theoretical models for electron dynamics in solids e.g. Time Dependent-Density Functional Theory (TD-DFT) (Quashieet al., 2021; Kononov and Schleife, 2021).

2. Experimental setup

All measurements of the specific energy loss were performed using the Time-of-Flight Medium Energy Ion Scattering System at the 350 keV Danfysik Implanter at the Uppsala University (Linnarssonet al., 2012; Sortica et al., 2020). Pulsed beams of H^+, H_2^+ and He^+ ions were directed towards the experimental chamber with energies ranging from 60 to 300 keV. Electrostatic chopping combined with a vertical gating pulse and several sets of slits located along the beamline resulted in a parallel pulsed beam with time resolution of ~1–3 ns, beam current on the target of 2–3 fA and a beam spot below $\sim 1 \times 1$ mm^2. Transmitted ions were detected by a large solid angle (0.13 sr), position-sensitive microchannel plate (MCP) detector located 290 mm behind the target. The detector has a diameter of 120 mm which corresponds to an angular diameter of 23°. The position of incident particles was obtained from two perpendicular delay lines while the time of flight signal was obtained from the MCP plate. The sample holder was positioned in the centre of the scattering chamber which features a 6-axis goniometer allowing the selection of different orientations of the crystal. The pressure in the experimental chamber was kept below 1×10^{-8} mbar during the course of all measurements.

The target was self-supporting, single-crystalline, cubic 3C polytype SiC (100) (Norcada Inc. (https://www.norcada.com/)) with nominal thickness of 200 nm. Rutherford backscattering spectrometry (RBS) was employed to confirm the areal thickness of the thin film using 2-MeV He^+ ions provided by the 5-MV 15SDH-2 Pelletron Tandem accelerator at Uppsala University. The detector was a passivated implanted planar silicon detector mounted at 170° with respect to the primary beam. The chosen sample geometry was 5° rotation around the y-axis and 0° rotation around the x-axis. These specific angles were chosen to minimize channeling effects which could potentially result in inaccuracies in the thickness measurement that would directly be propagated in the deduced stopping. In order to further suppress the channeling phenomena, during the course of the measurement, twelve small random angular movements around the equilibrium angle were performed within a range of 0.6° and with duration of 30 s per movement. In order to bypass the absolute calculation of the collected charge (Q) and the detector solid angle (Ω), a thick Cu target was also irradiated in between the SiC thickness measurements for 15 s per measurement. Following the completion of the measurements, the obtained spectra were examined for experimental effects related to channeling, added and analysed using the SIMNRA code (Mayer, 1999). The $Q \times \Omega$ term was obtained from the simulation of the Cu spectra and used in the evaluation of the SiC spectrum. The obtained foil thickness value was 196 nm with a relative uncertainty better that 5%. No specific sample cleaning was performed on-site for the present experiments since SiC is expected to become significantly oxidized only in a high temperature environment due to its excellent chemical inertia (Phanet al., 2017).

All data acquired from the MCP plate were evaluated using the acquisition software Cobold PC (Computer Based Online offline List-mode Dataanalyzer) (https://www.roentdek.com/). Details on how data are stored in Cobold PC along with different possible contrast modes can be found in (Holeňáket al., 2020). Fig. 1 shows the recorded 2D intensity distribution for He ions with a primary energy of 60 keV transmitted through the SiC (100) self-supporting foil. The [100] crystal axis of the SiC foil is aligned with the beam. In this alignment the majority of the ions are steered in the centre of the (100) channel by a series of small angle collisions, and impinges on the detector at small detection angle close to the projected trajectory of the incident beam. A minority of the ions is escaping the channel and impinges on the detector at deflection angles larger than the critical angle for channeling (Lindhard, 1965) (up to ±11.5°). These ions are exiting the crystal preferentially through the planes (planar scattering) forming a real-space image of the crystalline structure on the detector plane. Fig. 2 shows another 2D intensity distribution recorded for He ions with a primary energy of 60 keV, but in this case no crystal axis or plane of the SiC (100) membrane was aligned with the beam, resulting in a (pseudo-)random geometry. The foil was rotated 5° around the x-axis and 10° around the y-axis with respect to the channelling geometry. This rotation resulted in a distribution where the majority of the ions are exiting the crystal from the planes and channels closest to the incident beam position. It can be observed that the ions, initially impinging on the crystal in a random position, were eventually steered into the surrounding planes and channels and exit the crystal from them, even though the axes of these channels can be located as far as ±12° from the primary beam orientation. For every beam energy, energy loss measurements were performed in both channeling and random orientation.

2.1. Data analysis

The time of flight spectra, acquired by the detector, were converted to energy spectra using the Cobold PC. We evaluated ions transmitted along rather straight trajectories, by selecting small circular regions of interest (ROI) around the initial beam position for random geometries and around the channel position for channeling geometries. These ROIs, visible in both Figs. 1 and 2, had 4 mm radii corresponding to deflection

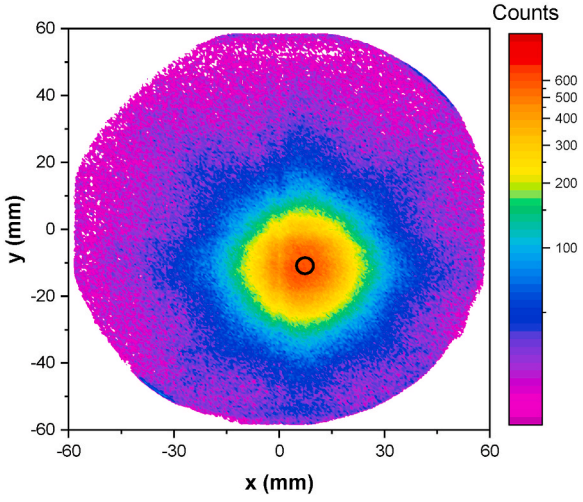

Fig. 1. 2D intensity distribution of 60 keV primary energy He^+ transmitted through a 200 nm SiC (100) self-supporting foil. The crystal axis [100] of the SiC foil is aligned with the beam. The black circle indicates the evaluated region of interest in channeling orientation.

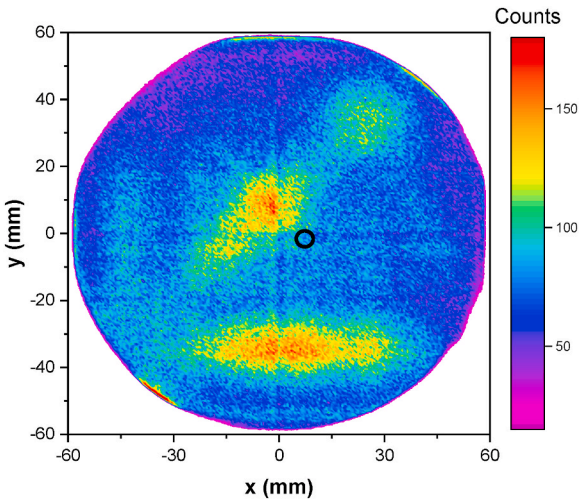

Fig. 2. 2D intensity distribution of 60 keV primary energy He^+ transmitted through a 200 nm SiC (100) self-supporting foil. In contrast to Fig. 1 the membrane is turned $R_x = 5°$ around the x-axis and $R_y = 10°$ around the y-axis with respect to the channeling alignment from Fig. 1. All other experimental conditions remained the same. The black circle indicates the evaluated region in random orientation. The faded cross visible in the centre of the 2D intensity distribution is an artifact from the Cobold PC software.

angles of ±0.8°. Subsequently, the energy loss spectra were obtained by subtracting the final energy of the ions from the initial energy. The energy loss spectra for He ions with primary energy 60 keV are shown in Fig. 3 for both random and channeling orientations. The curves are normalized to their respective maxima for comparison purposes. Apparently, the ions lose less energy along the channeled trajectory. Both curves qualitatively have a Gaussian distribution, although an asymmetry (tail at the high energy loss side) can be observed. Such tail is attributed to the gradually increasing energy loss for larger angles and potential minor contributions from nuclear energy loss, but displays minimum effect on the centroid position of each peak. The energy loss value for each geometry is thus determined via the centroid value of the corresponding peak fitted with a Gaussian function, visible in Fig. 3. The measured energy loss is expected to correspond only to electronic energy loss. No subtraction of the nuclear energy loss was deemed necessary since in the case of 60 keV He with random incidence on SiC, in which the most significant contribution to the total energy loss is expected, we calculated 2% elastic losses using SRIM (Ziegleret al., 2010). Moreover, since only straight ion trajectories were selected during the evaluation process (i.e. avoiding close collisions with target nuclei), the nuclear energy loss contribution is expected to be even lower than predicted by SRIM (Naqviet al., 2016).

To calculate the electronic stopping cross section values from the energy loss, the thickness of the SiC target and the gradual change in ion energy, and thus electronic stopping must be considered. For this, we employed a numerical integration procedure: the target was divided into 20 slabs and for each one of these slabs we assumed a velocity dependent stopping power in accordance with predictions from SRIM applying a constant correction factor. The stopping value was determined when the calculated total energy loss in the target, namely the sum of the energy losses from each one of these slabs, resulted in the same value as the measured energy loss. This numerical integration procedure was performed iteratively until convergence was achieved, i.e. the resulting stopping cross sections were again fitted by a function parametrized according to SRIM, and this fit function in turn employed for repeated reevaluation of the data.

3. Results and discussion

The specific energy loss is compared with SRIM predictions (Ziegler et al., 2010) and previously measured datasets in Fig. 4 for the H projectiles and in Fig. 5 for the He projectiles. In both figures, the blue filled dots denote electronic stopping power values measured in random orientation whereas the red filled diamonds correspond to the [100]-channeling geometry. The uncertainty bars include the statistical uncertainties in the peak fitting procedures, potential systematic uncertainties in distance between target and detector, because of the rotation of the crystal, and the time resolution. The systematic uncertainty of target thickness from RBS is not included. In Fig. 4, for H projectiles, the present data for random geometries, for higher energies, agree within quoted errors with SRIM predictions as well as with the theoretical predictions from Heredia – Avalos et al. (Heredia-Avalos et al., 2005). Closer to the stopping maximum our data agree with the ones measured by Linnarsson et al. (Linnarsson et al., 2014) revealing

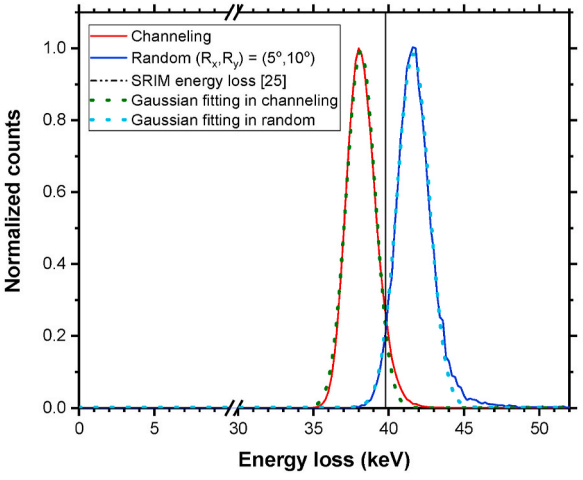

Fig. 3. Energy loss spectra of He^+ transmitted through a 200 nm SiC (100) self-supporting foil. The initial ion energy is 60 keV and data are taken from the circular region of interest with 4 mm radius for each measurement. Both curves are normalized to the maximum of each measurement. The vertical black line is the energy loss value for amorphous SiC from SRIM (Ziegler et al., 2010) while the dotted lines correspond to the fittings of Gaussian distributions to the corresponding energy loss peaks.

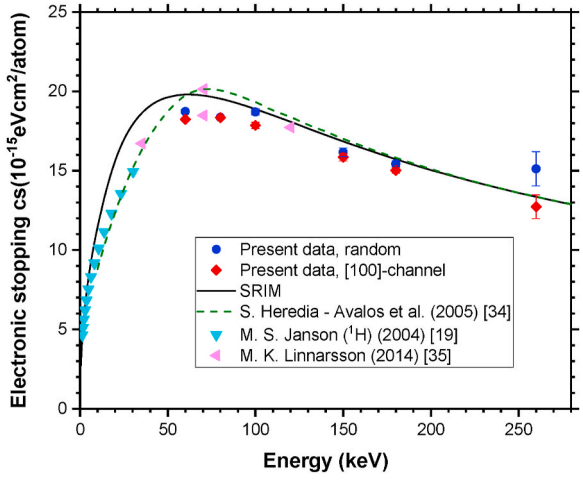

Fig. 4. Electronic stopping cross sections (10^{-15}eV cm^2/atom) of SiC for H ions measured in transmission geometry. H ions were transmitted through a single crystalline SiC (100) self-supporting foil. The blue filled dots correspond to a random geometry whereas the red filled diamonds correspond to a channeling geometry. The present data are presented along with SRIM predictions, theoretical predictions from Heredia – Avalos et al. and previously measured datasets.

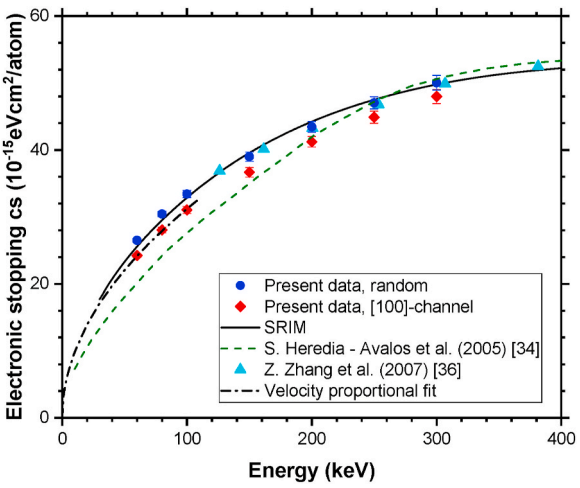

Fig. 5. Electronic stopping cross sections (10^{-15}eV cm^2/atom) of SiC for He ions measured in transmission geometry. He ions were transmitted through a single crystalline SiC (100) self-supporting foil with nominal thickness of 200 nm. Symbols are the same as in Fig. 4. SRIM predictions along with theoretical predictions from Heredia – Avalos et al. and previously measured datasets are also included. The dash-dotted line corresponds to a linear fit to our stopping cross sections (up to 100 keV) as a function of velocity in channeling geometry.

values slightly lower than the SRIM data. The measured stopping maximum (at ~60 keV) confirms the predictions by SRIM. In channeling orientation, the stopping displays lower values than the random orientation for all measured energies, as expected since the channeled ions have a small probability of a close encounter with the atoms. Differences in the stopping values between random and channeling geometry are minor (up to 4%) within the measured energy range except for the highest energy data point (260 keV), where also the largest uncertainties in ToF are involved. In Fig. 5, for He projectiles, electronic stopping powers from SRIM agree well with our experiment, whereas theoretical predictions from Heredia – Avalos et al. have an evidently different slope. The agreement with the dataset from Zhang et al. (Zhang et al., 2007), also measured in transmission with a self-supporting single crystalline SiC in random geometry, is excellent. Our data extends the range of energies for which data is available by a factor of 2 towards lower values. Differences in stopping cross sections between random and channeling orientations for He ions are found more pronounced than for H ions, although they remain below 10% for all measured energy values, i.e. smaller than earlier observed for Si (Lohmann and Primetzhofer, 2020).

As expected, electronic stopping cross sections in SiC in random geometry display values higher than in carbon (SRIM values) and lower than in amorphous silicon (SRIM values), for both projectiles within the studied energy range. Concerning the channeling orientation, 3C–SiC features narrower channels in comparison to Si in similar orientation since it exhibits a higher atomic density (~10×10^{22} at/cm^3) than Si (~5×10^{22} at/cm^3). This fact implies, that the maximum impact parameters probed will be significantly smaller in SiC than in Si in channeling geometry. As the difference in stopping between random and channeling geometry is attributed to additional losses associated with small impact parameter collisions, this could help to understand the smaller differences between different sample orientations in SiC than observed for Si. In this context, considering the presence of C in SiC, exceptional neutralization and reionization behavior along the trajectories could be expected while interacting with He ions (Mikhailov et al., 1994). In LEIS geometries, it was found, that C can ionize neutral He ions with energies of about 200 eV while the threshold for Si is 400–500 eV (Brongersma et al., 2007). For the present energies, this implies that for C, a deflection of only 0.12° would correspond to an impact parameter at which charge exchange processes can occur. For Si, in comparison a scattering angle of around 0.28° is necessary (scattering angles calculated using (Schmid, 2002–2013)). The presence of such charge changing collisions can yield an additional contribution to the energy loss and, potentially even more important affects the mean charge state, which in turn influences the efficiency of electron hole pair excitation along the trajectory – and might be accessible to a very different extend along channeling trajectories in the case of SiC in comparison to Si. Note, that the effects of these processes are expected to show a complex dependence on energy, as the interaction time is of critical importance, different distances of closest approach are reached for given deflection angles at different energies and mean charge states decrease with lower energy (Primetzhofer et al., 2013; Arnau et al., 1990; Primetzhofer, 2012; Holenak et al., 2020).

For the lowest investigated energies, at least for the case of He, stopping is expected to be proportional to velocity for a free electron gas (FEG), but deviations have been observed dependent on the target electronic structure as well as due to contributions from charge exchange processes (Arnau et al., 1990; Primetzhofer, 2012; Markin et al., 2009a). A dash-dotted line in Fig. 5 indicates a velocity proportional stopping cross section fitted to our data in channeling direction up to 100 keV ($v = v_0$). This velocity proportionality proves that SiC can be considered a FEG for the lower measured energies. In this framework, it should also be stressed here that SiC is a wide band gap semiconductor (2.3 eV for 3C–SiC) also in comparison to Si, which has a band gap of 1.1 eV. For large band gap materials, strong deviations from velocity proportionality have been observed at low ion energies (Draxler et al., 2005; Markin et al., 2009b; Primetzhofer et al., 2011b). These observations were however made at much lower energies than initially predicted (Fermi and Teller, 1947; Eder et al., 1997). Therefore, a future comparison of stopping measurements for SiC in channeling geometry to those of Si at even lower projectile energies based on the present study can shed new light on the detailed influence of the electronic structure on electronic energy dissipation by charged particles in matter.

4. Summary and conclusions

Electronic stopping cross sections have been determined by measuring the energy loss of H and He ions in self-supporting, membranes of single-crystalline SiC (100) in an energy range of 60–300 keV in both channeling and random orientations. The obtained results were compared with SRIM, theoretical predictions for stopping and measured datasets from literature. For H ions, the difference between stopping in random and channeling trajectories is minor, while slightly lower values than predicted by SRIM were measured. For He ions, our stopping data agree with SRIM, theoretical predictions from Heredia – Avalos et al. for energies above 200 keV and measured data from Zhang et al. while differences between the two geometries are generally more pronounced. The comparison of experimental data in different orientations with well-defined impact parameters accessed in the respective geometry could be of advantage for developing and benchmarking dynamic theoretical models. Moreover, it will help to obtain a better understanding of the specific contributions of target electronic structure and dynamic processes such as formation of molecular orbitals and charge exchange to the energy loss.

Author statement

Eleni Ntemou: Investigation, Visualization, Formal analysis, Data Curation, Methodology, Writing - Original Draft **Radek Holeňák**: Investigation, Methodology, Data Curation, Writing - Review & Editing **Daniel Primetzhofer**: Conceptualization, Resources, Writing - Review & Editing, Supervision, Project administration, Funding acquisition.

Declaration of competing interest

The authors declare that they have no known competing financial

interests or personal relationships that could have appeared to influence the work reported in this paper.

Acknowledgements

Accelerator operation is supported by the Swedish Research Council VR-RFI (Contracts No. 2017-00646_9 and 2019-00191), the Swedish Research Council VR (Contracts No. 2016-03432 and 2020-04754) and the Swedish Foundation for Strategic Research (Contract No. RIF14-0053).

References

Andersen, H.H., et al., 1977. Nuclear Instr. Meth. Phys. B 140 (3), 537.
Arnau, A., et al., 1990. Phys. Rev. Lett. 65 (8), 1024.
Barkas, W.H., et al., 1963. Phys. Rev. Lett. 11, 26.
Bethe, H.A., 1930. Ann. Phys. 5, 325.
Bragg, W.H., Kleeman, R., 1905. The London, Edinburgh, and Dublin Philosophical Magazine and Journal of Science 10 (57), 318–340. https://doi.org/10.1080/14786440509463378.
Brandt, W., et al., 1973. Phys. Rev. Lett. 30 (9), 351.
Brongersma, H.H., et al., 2007. Surf. Sci. Rep. 62, 63.
Bruzzi, M., et al., 2001. Appl. Surf. Sci. 184, 425–430.
Draxler, M., et al., 2005. Phys. Rev. Lett. 95, 113201.
Durante, M., et al., 2017. Nat. Rev. Clin. Oncol. 14, 483.
Eder, K., et al., 1997. Phys. Rev. Lett. 79, 21.
Fermi, E., Teller, E., 1947. Phys. Rev. 72, 5.
Han, Y., et al., 2020. Compos. Sci. Technol. 187, 107944.
Heredia-Avalos, S., et al., 2005. Nuclear Instr. And Meth. In Physics B 230, 118. Issues 1-4.
Holeňák, R., et al., 2020. Ultramicroscopy, 113051.
Holenak, R., et al., 2020. Vacuum 185, 109988.
https://www-nds.iaea.org/stopping/.
https://www.norcada.com/.
https://www.roentdek.com/.
Janson, M.S., et al., 2004. J. Appl. Phys. 96, 164.
Kononov, A., Schleife, A., 2021. Nano Lett. 21, 4816.
Lindhard, J., 1965. Mat. Fys. Medd. Dan. Vid. Selsk. 34. No. 14.
Lindhard, J., Scharff, M., 1953. Mat. Fys. Medd. K. Dan. Vidensk, Selesk 27 (15).
Linnarsson, M., et al., 2012. Rev. Sci. Instrum. 83, 095107.
Linnarsson, M., et al., 2014. Nuclear Instr. And Meth. In Physics B 332, 130.
Lohmann, S., Primetzhofer, D., 2020. Phys. Rev. Lett. 124, 096601.
Markin, S.N., et al., 2009a. Phys. Rev. B 80, 205105.
Markin, S.N., et al., 2009b. Phys. Rev. Lett. 103, 113201.
Mayer, M., 1999. Am. Inst. Phys. Conf. Proc. 475, 541.
Mikhailov, S.N., et al., 1994. Nuclear Instr. And Meth. In Physics B 93, 210.
Naqvi, S.R., et al., 2016. Nuclear Instr. And Meth. In Physics B 371, 76.
Phan, H.P., et al., 2017. ACS Appl. Mater. Interfaces 9 (33), 27365.
Primetzhofer, D., 2012. Phys. Rev. B 86, 094102.
Primetzhofer, D., et al., 2011a. Phys. Rev. Lett. 107, 163201.
Primetzhofer, D., et al., 2011b. Nuclear Instr. And Meth. In Physics B 269, 2063.
Primetzhofer, D., et al., 2013. Nuclear Instr. And Meth. In Physics B 317 (Part A), 8.
Puglisi, D., Bertuccio, G., 2019. Micromachines 10 (12), 835.
Quashie, E.E., et al., 2021. European Physics Journal D 75, 280.
Riccardi, P., et al., 2017. Phys. Lett. 381, 1174.
Roccaforte, F., et al., 2018, 187-188 Microelectron. Eng. 66.
Schmid, M., 2002-2013. LEIS Energy Calculator. IAP/TU Wien Surface Physics Group (Data retrieved 09/11/2021. https://www.iap.tuwien.ac.at/www/surface/leis.
Sortica, M.S., et al., 2020. Nuclear Instr. And Meth. In Physics B 463, 16.
Vajdi, M., et al., 2020. Ceram. Int. 46, 21775–21783.
Handbook of Modern Ion Beam Analysis Materials Analysis, second ed., Editors: Y. Wang, M. Nastasi.
Werner, M.R., et al., 2001. IEEE Trans. Ind. Electron. V. 48 (No. 2), 249.
Zhang, Z., et al., 2007. Nuclear Instr. And Meth. In Physics B 261, 1180.
Zhang, Z., et al., 2021. Comput. Mater. Sci. 190, 110267.
Ziegler, J.F., et al., 2010. Nuclear Instr. And Meth. In Physics B 268, 1818.